Integration of chemical looping combustion for cost-effective CO_2 capture from state-of-the-art natural gas combined cycles

Mohammed N. Khan[a,b], Paolo Chiesa[c], Schalk Cloete[d,*], Shahriar Amini[a,d,*]

[a] Norwegian University of Science and Technology, Trondheim, Norway
[b] Flemish Institute for Technological Research (VITO), Mol, Belgium
[c] Department of Energy, Politecnico di Milano, Milan, Italy
[d] SINTEF Industry, Trondheim, Norway

ABSTRACT

Chemical looping combustion (CLC) is a promising method for power production with integrated CO_2 capture with almost no direct energy penalty. When integrated into a natural gas combined cycle (NGCC) plant, however, CLC imposes a large indirect energy penalty because the maximum achievable reactor temperature is far below the firing temperature of state-of-the-art gas turbines. This study presents a techno-economic assessment of a CLC plant that circumvents this limitation via an added combustor after the CLC reactors. Without the added combustor, the energy penalty amounts to 11.4%-points, causing a high CO_2 avoidance cost of $117.3/ton, which is more expensive than a conventional NGCC plant with post-combustion capture ($93.8/ton) with an energy penalty of 8.1%-points. This conventional CLC plant would also require a custom gas turbine. With an added combustor fired by natural gas, a standard gas turbine can be deployed, and CO_2 avoidance costs are reduced to $60.3/ton, mainly due to a reduction in the energy penalty to only 1.4%-points. However, due to the added natural gas combustion after the CLC reactor, CO_2 avoidance is only 52.4%. Achieving high CO_2 avoidance requires firing with clean hydrogen instead, increasing the CO_2 avoidance cost to $96.3/ton when a hydrogen cost of $15.5/GJ is assumed. Advanced heat integration could reduce the CO_2 avoidance cost to $90.3/ton by lowering the energy penalty to only 0.6%-points. An attractive alternative is, therefore, to construct the plant for added firing with natural gas and retrofit the added combustor for hydrogen firing when CO_2 prices reach very high levels.

1. Introduction

Anthropogenic carbon dioxide (CO_2) emissions have increased to a record level of 415 ppm in the atmosphere [1]. Even though CO_2 emissions growth has slowed in recent years, the world is still on track to strongly overshoot the recommended 1.5–2 °C global temperature rise window [2]. In addition to energy efficiency, renewables, and nuclear power, carbon capture and storage (CCS) will be required to achieve the rapid CO_2 reductions recommended by climate science [3].

However, CCS integrated with conventional power plants poses a considerable energy penalty (~8%-points) [4–6]. Large energy penalties increase the fuel costs and the capital costs of a plant relative to a reference plant of the same power output. The reduction of the energy penalty is, therefore, an important research focus in the field of CO_2 capture.

Chemical looping combustion (CLC) integrated with a combined cycle power plant inherently captures CO_2 with minimum energy penalty [7]. As the fuel and oxidizer (air) are reacted separately, a pure CO_2 stream with condensable water is obtained. The reactions occur in separate reactors by circulating a metal oxide oxygen carrier (OC). The fuel reacts with the OC in a reduction reaction in the fuel reactor (FR) followed by an oxidation reaction between the air and the OC in the air reactor (AR). The generalized chemical reactions in the two reactors are shown below.

Reduction: $4MeO + CH_4 \rightarrow 4Me + 2H_2O + CO_2$ (1)

Oxidation: $4Me + 2O_2 \rightarrow 4MeO$ (2)
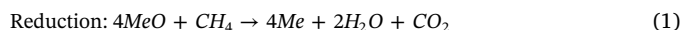
The CLC process is similar to a standard oxy-fuel process wherein the use of an OC material significantly reduces the energy penalty of air separation [8]. However, due to the OC material limitations, the CLC reactor temperatures are also limited. In a CLC combined cycle plant, the AR outlet stream is expanded in the gas turbine for power

---

Nomenclature

AC	Air compressor
AS	Air section
CAC	CO_2 avoidance costs
CCS	Carbon capture and storage
CFB	Circulating fluidized bed
CLC	Chemical looping combustion
CLR	Chemical looping reforming
COMB	Combustor
COND	Condenser
COT	Combustor outlet temperature
CT	Cooling tower
EBTF	European benchmark task force
EX	Expander
FS	Fuel section
GPSA	Gas processors suppliers association
GT	Gas turbine
GTCC	Gas turbine combined cycle
HP	High pressure
HRSG	Heat recovery steam generator
ICR	Internally circulating reactor
IP	Intermediate pressure
LHV	Low heating value
LP	Low pressure
MA-CLR	Membrane-assisted chemical looping reforming
MEA	Monoethanolamine
NG	Natural gas
NGCC	Natural gas combine cycle
OC	Oxygen carrier
PH	Preheater
PCC	Post combustion capture
RKS-BM	Redlich-Kwong-Soave-Boston-Mathias
SC	Steam cycle
SPECCA	Specific primary energy consumption for CO_2 avoided
ST	Steam turbine
TIT	Turbine inlet temperature

---

production while the FR outlet stream is used to produce steam in a heat recovery process. The AR outlet temperature corresponds to the combustor outlet temperature (COT) of a standard oxy-fuel or natural gas combined cycle (NGCC) plant. Owing to lower reactor temperatures, the power production efficiency is reduced and low-quality heat recovery is obtained. Despite intensive research on the development of temperature resistant OC materials [9], the temperature limitation of the process is constrained in the range 800–1200 ℃ [10].

Pressurization of the CLC process is another challenge in achieving competitive energy efficiencies. Several reactor configurations ranging from a dual circulating fluidized bed (CFB) [11] to a dual bubbling fluidized bed [12] have been employed for the conventional CLC process. These configurations have been demonstrated experimentally both at the lab- and pilot scales and mostly under atmospheric pressures [13–15]. However, the scale-up of these configurations at pressurized conditions presents technical challenges associated with solids circulation rate and gas leakages between the two reactors. Thus, several reactor configurations have been proposed to simplify this scale-up challenge such as gas switching packed/fluidized bed [16] and rotary reactor configuration [17]. These configurations can simplify pressurized operation but introduce other technical challenges. The transient nature of the gas switching process using high-temperature switching valves and the significant gas leakages in the rotary configuration are some of the key disadvantages of these concepts. On the contrary, the dual CFB operation is steady with relatively low gas leakage and thus, remains attractive despite the challenges in solid circulation and pressurized operation.

The scale-up challenges of this configuration under pressurized conditions can be reduced by simplifying the solids circulation mechanism. Therefore, a novel reactor configuration named internally circulating reactor (ICR) is proposed where the two CFB reactors along with the cyclones and loop seals are combined into a single reactor that can be pressurized within a single pressure shell. This reactor is divided into two sections – a fuel section and an air section connected by two simple ports. The ports replace the complex system of cyclones and loop seals and are specially designed for steady solids circulation. The schematic of the ICR configuration is shown in Fig. 1 with the arrows indicating the movement of the solid particles. The solids circulation is achieved by maintaining a higher superficial gas velocity in the air section than the fuel section.

Kuramoto et al. [18] first proposed the concept of an internally circulating reactor. The objective of the study was to develop a single vessel reactor that has the same advantages as that of a dual CFB in the fluid catalytic process (FCC). They concluded that this reactor could

also be employed for gasification of biomass and other solid wastes. Barisano et al. [19] utilized the ICR concept in biomass gasification by using steam and oxygen (O_2). The results showed a significant increase in the cold gas efficiency from 0.5 to 0.7. Li et al. [20] utilized the advantages of the ICR principle in producing polysilicon granules. They conducted a numerical hydrodynamic study by varying parameters such as gas velocity and particle diameter that affect the silicon deposition on the walls.

Owing to the advantages of the ICR concept, it is well suited for chemical looping processes. Zaabout et al. [21] carried out a detailed hydrodynamic study on a pseudo-2D experimental setup and identified the most influential operating parameters. It was concluded that the solids circulation rate was easy to control by changing the fluidization velocity ratio. However, large fluidization velocity ratios created large
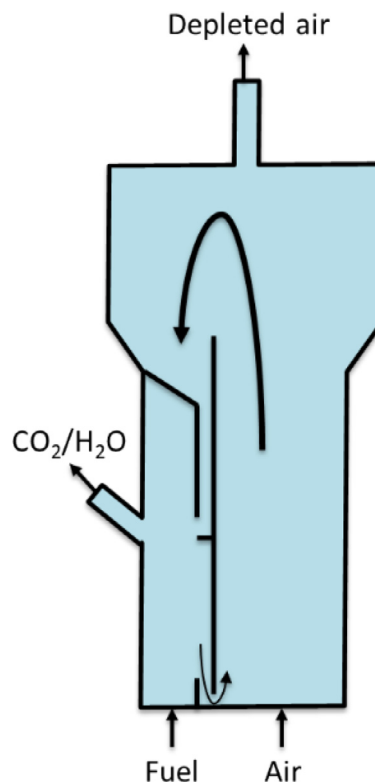

Fig. 1. Schematic of an internally circulating reactor.

pressure imbalances that resulted in high gas leakages. A gas/solids leakage ratio of 2 was found over a wide range of fluidization velocities and bed loadings. This corresponds to high CO_2 capture efficiency and high CO_2 purity of up to 95% for the CLC process. With the experience from these experiments, Cloete et al. [22] developed a numerical reactive multiphase flow model of a large-scale (100 MWth) reactor employing an iron-based oxygen carrier. The performance of the ICR concept in chemical looping processes such as combustion, reforming, oxygen production and water splitting was investigated. The results showed that CO_2 capture and purity of above 96% could be obtained for all the processes except water splitting (CO_2 purity of 90%). Recently, Osman et al. [23] demonstrated the chemical looping reforming (CLR) process on a dedicated ICR experimental rig with a nickel-based oxygen carrier. It was observed that methane was converted to syngas with an efficiency as high as 98%. It was also concluded that the autothermal operation of the ICR could be achieved, demonstrating the practicality of the concept. Chemical looping combustion was also demonstrated in the ICR recently over a wide range of flow rates and OC loadings [24].

With good CO_2 separation and purity, combined with ease of solids circulation control, the ICR concept can accelerate the scale-up of CLC technology. However, for successful commercial deployment, the concept should be economically viable. In this respect, CLC faces an important fundamental problem: the maximum operating temperature of the reactor will always be far below the firing temperature of modern gas turbines. Many authors [25–29] have simulated CLC-based natural gas power plants, mostly reporting efficiencies (LHV) in the low 50%-range. This translates into an unacceptably large energy penalty in excess of 10%-points relative to state-of-the-art NGCC power plants. In terms of economics, the present authors have recently shown that reactor temperatures of 1150 °C result in a process that is only on par with more technologically mature post-combustion CO_2 capture [30]. It was shown that higher reactor temperatures can substantially improve economic performance, but it is doubtful whether the oxygen carrier material, reactor body, and downstream particle filters will be able to operate reliably at temperatures considerably higher than 1150 °C.

To address this fundamental problem, the present authors have recently proposed the introduction of an added combustor downstream of the CLC reactor [31]. However, the aforementioned study used a relatively outdated NGCC benchmark plant with simplified modeling of the gas turbine. State-of-the-art NGCC plants use sophisticated gas turbines with very high firing temperatures and a large amount of cooling on the turbine blades. The present study will, therefore, evaluate the concept of added firing after the CLC reactor using detailed modeling of a state-of-the-art gas turbine. The ICR concept will be used as the CLC unit to facilitate a simplified scale-up. Performance indicators such as net electrical efficiency, CO_2 avoidance, levelized cost of electricity (LCOE) and CO_2 avoidance costs will be determined and compared with a state-of-the-art reference NGCC plant with and without CO_2 capture.

2. Methodology

The following sections present the process description of the reference NGCC plant with (NGCC-PCC) and without post-combustion CO_2 capture (NGCC), a base case ICR combined cycle plant (ICR-CC), an ICR combined cycle plant with an NG-fired combustor (ICR-NG), an ICR combined cycle plant with a H_2-fired combustor (ICR-H_2) and an ICR combined cycle plant with a steam-diluted H_2-fired combustor (ICR-H_2-2P).

2.1. Process description

In the current study, one standard H-class gas turbine with a heat recovery steam generator (HRSG) and a steam turbine (ST) is considered in all cases, except for the ICR-CC case. In this particular case, due to the low COT, the turbine is simulated in Aspen Plus with the GE 9371FB gas turbine specifications as discussed in our previous work

Table 1
Performance specs of the H-class gas turbine operating in a combined cycle configuration. Operating conditions are those summarized in Table 2.

Gross generator output, MW	520
Fuel thermal input (LHV), MW	1209
Fuel temperature at combustor inlet, °C	220
Air mass flow rate at the compressor inlet, kg/s	947.6
Compressor pressure ratio	23.6
TIT (Total temperature at 1st rotor inlet), °C	1550
Exhaust gas temperature, °C	641

[31]. Specifications of the H-class gas turbine are summarized in Table 1 and have been assumed to reflect the average performance of state-of-the-art, commercially available, heavy-duty units [32].

However, in the ICR cases with added firing, the turbine is operated under off-design mode at a lower pressure ratio and a lower power output. Off-design operation is required because the flowrate through the expander is reduced as the ICR extracts some CO_2 and H_2O from the combustion gases stream. The turbine is modeled in detail using an in-house code conceived for the prediction of gas turbine performance at the design point [33]. It performs the one-dimensional design of the turbine, aimed at establishing all the aerodynamic, thermodynamic, and geometric characteristics of each blade row. Proper correlations are then applied for the evaluation of the efficiency of the stages, while an accurate estimation of the blade cooling flow rates is considered by a model accounting for convective cooling in multi-passage internal channels with enhanced heat transfer surfaces, as well as film and Thermal Barrier Coating (TBC) cooling.

Fig. 2 shows the schematic of the NGCC reference plant. In this system, the air enters the combustor at a pressure of 23.74 bar. The total air flow rate is 947.6 kg/s, of which ~22% is extracted for turbine blade cooling. The natural gas at a flowrate of ~26 kg/s and a pressure of 35 bar is preheated to a temperature of 220 °C before entering the combustor. The COT is 1647.8 °C, which, after mixing with the cooling air, results in the TIT of 1550 °C at the first rotor. The high-temperature outlet stream is expanded in the gas turbine to near atmospheric pressure followed by heat recovery from the exhaust stream at a temperature of 641 °C in a steam cycle. A triple pressure HRSG is employed that produces high pressure (HP) steam at 185 bar, intermediate pressure (IP) steam at 43 bar and low pressure (LP) steam at 6 bar. The steam is expanded in the ST assembly for additional power generation. The gas turbine is simulated using the in-house code described above, while the steam cycle consisting of HRSG, ST, condenser (COND), and natural draft cooling tower (CT) are simulated in the Thermoflex component of the Thermoflow suite [34]. This is consistent in all the cases considered in this study. An NGCC combined cycle plant with a post-combustion capture system (NGCC-PCC) based on mono-ethanolamine (MEA) with a typical capture efficiency of 90% was also simulated. The detailed process description of the MEA-based capture system can be found in Ref. [35]. The post-combustion CO_2 capture module available in Thermoflex was used in the current study [34]. The plant specifications and the main assumptions are listed in Table 1.

Fig. 3 shows the schematic of the ICR unit integrated with a combined cycle power plant and an additional H_2-fired combustor (ICR-H_2). The base case ICR combined cycle plant (ICR-CC) is similar, although the H_2 supply and the added combustor (COMB) are removed. More details are given in our previous work [31].

The ICR unit replaces the combustor of the NGCC plant. As mentioned earlier, the ICR operates similar to conventional CLC but without cyclones and loop seals. These components are replaced by simple ports, which are modeled by using a separator block with the leakage ratio specified. The leakage ratio is obtained from the computational fluid dynamics (CFD) simulations reported in our previous study, which indicated CO_2 capture efficiency and purity of 95% [30]. This previous detailed simulation study, as well as experimental studies in an ICR [23], have shown that a simplified reactor model assuming complete
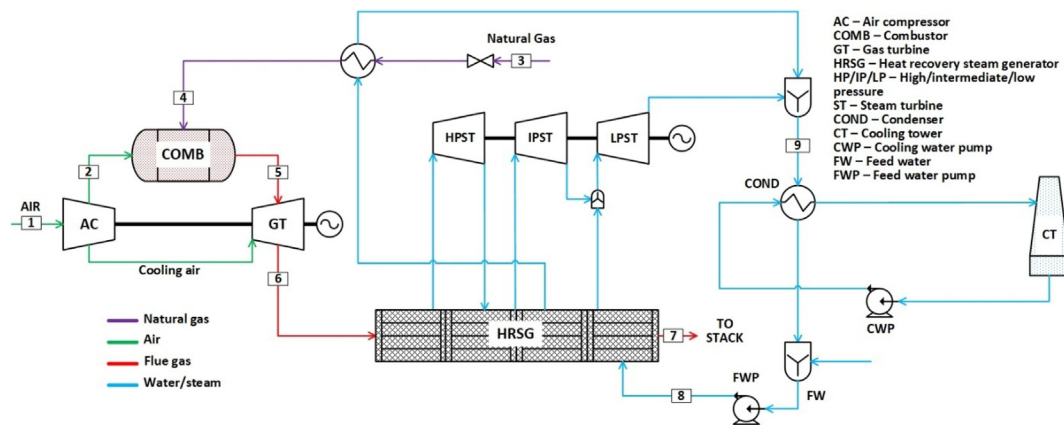
Fig. 2. Process flow sheet of the natural gas combined cycle power plant.

fuel conversion is reasonable due to the high reactivity of the oxygen carrier. The ICR unit is divided into a fuel section (FS) and an air section (AS). In the FS, the reduction reaction takes place between the natural gas and the OC (NiO supported on $NiAl_2O_4$) whereas, in the AS, the oxidation reaction occurs between the reduced OC and the air. The FS outlet stream, consisting of CO_2 and H_2O, is expanded for power generation followed by fuel preheating (PH1). The CO_2 rich stream after condensation is then compressed to 110 bar and cooled to 30 °C to a supercritical state for storage.

The ICR-NG case is identical to the schematic shown in Fig. 3, only without the H_2 supply line. The NG was preheated to 440 °C using the CO_2 stream and split between the ICR and the added combustor.

It is a considerable benefit that the ICR plant with added firing can utilize the state-of-the-art gas turbine. However, the design of the added combustor is one point of uncertainty in the proposed plant, but it also presents an opportunity for high-temperature-low-NOx fuel combustion. Given that the depleted air stream exits the ICR at 1160 °C, the added combustor does not need to maintain a flame using a near-stoichiometric air/fuel ratio. Any fuel that is injected into this very hot oxidant stream will spontaneously combust, allowing the fuel to be fed directly into this large stream of excess air. In the limit of either an

infinite number of fuel injection points or infinite mixing, this added combustor will behave as an ideal lean premixed combustor. Thus, a combustor designed with multiple small injection nozzles can result in simple and efficient fuel combustion with very low NOx formation. Such a combustor is similar to the concept of MILD combustion [36] that has enjoyed considerable research attention in recent years due to its potential for higher efficiency and lower pollutant emissions. In the present study, it is assumed that such a combustor can be utilized successfully for both NG and H_2 added firing.

Fig. 4 shows the schematic of the ICR combined cycle plant and an additional combustor fired by H_2 with additional steam. This strategy was used to increase the gas volume flow in the turbine resulting in increased power production close to design conditions and to avoid expanding the CO_2 stream before having to compress it again. The water is pumped to 35 bar and mixed with the H_2 fuel. This gas-liquid mixture allows the water to start evaporating at low temperatures so that the condensation enthalpy from the steam in the pressurized CO_2 stream exiting the ICR can be used to efficiently raise this steam. The CO_2 expander was not considered in this case, allowing the mixture to be preheated to 800 °C using the CO_2 stream in this two-phase flow heat exchanger (2-PH) before injecting into the combustor. After removing
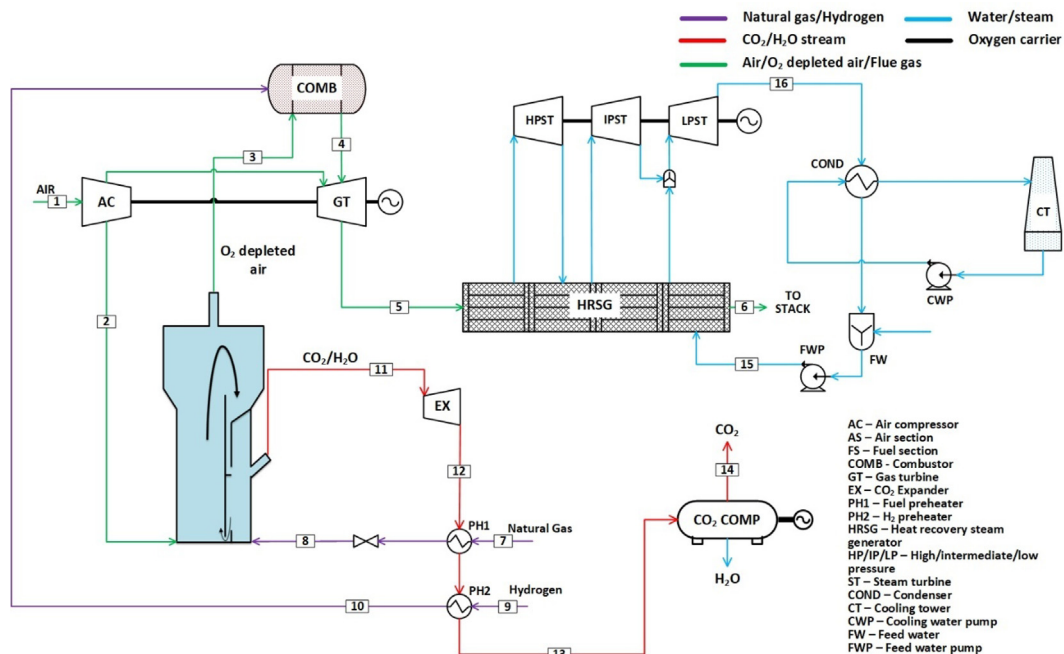

Fig. 3. Process flow sheet of the ICR combined cycle plant with an additional H_2-fired combustor.
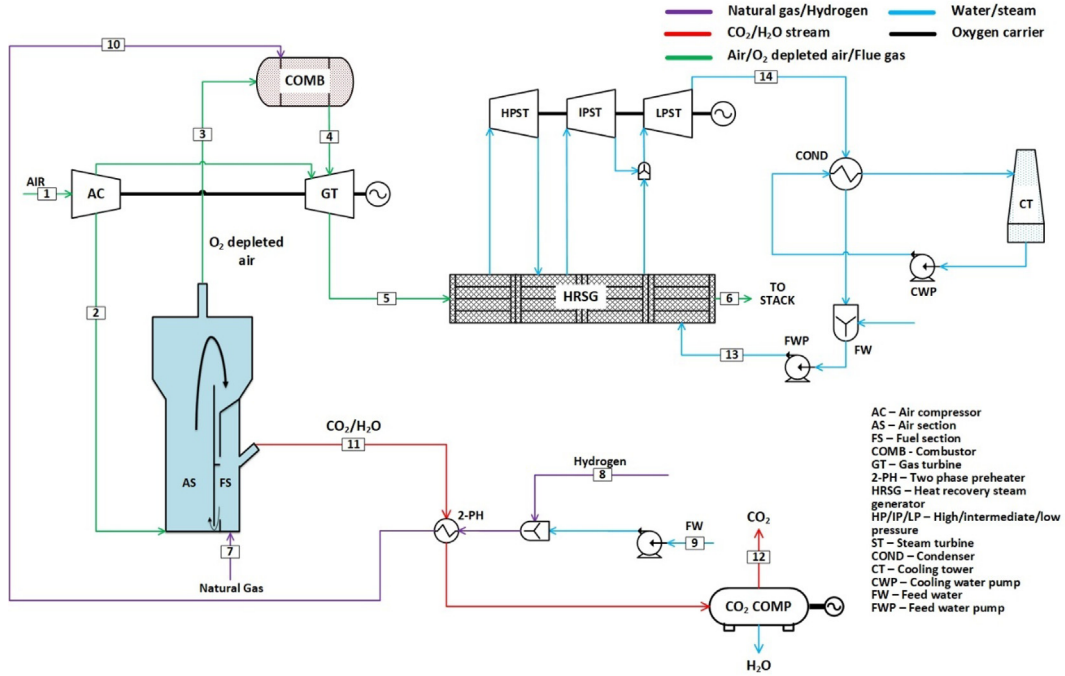
Fig. 4. Process flow sheet of the ICR plant with an additional combustor and two-phase flow heat exchanger (ICR-H2-2P).

the condensed water, the CO_2 stream was then sent for compression.

2.2. Process modeling assumptions and performance indicators

Thermodynamic equilibrium is assumed for the energy and mass balance calculations. The properties are evaluated using the Redlick-Kwong-Soave equation of state with Boston-Mathias alpha function (RKS-BM) as it is recommended for hydrocarbon processing applications [37]. The AS and the FS of the ICR unit are modeled separately using the RGIBBS module based on the Gibbs energy minimization concept. The ports are modeled as simple separators with gas leakages obtained from CFD simulations [30]. The efficiencies of compressors and expanders other than the main H-class gas turbine are evaluated using the polytropic with gas processors suppliers association (GPSA) method and are listed in Table 2. A condensing reheat steam turbine assembly is considered for power generation from heat recovery. The steam cycle assumptions are typical of those adopted in recent plants and are taken from Ref. [38]. A water-based natural draft cooling tower is adopted for the cooling required in the condenser.

The plant performance of all the cases in the present study is evaluated by using net electrical efficiency (%), efficiency penalty (%-points), CO_2 capture efficiency (%), CO_2 avoidance (%) and specific primary energy consumption for CO_2 avoided (MJ/kg) as shown below.

Net electrical efficiency: $\eta_{net} = \dfrac{\dot{W}_{net}}{\dot{m}_{fuel} * LHV_{fuel}}$ (3)

Efficiency penalty: $\eta_{pen} = \eta_{ref} - \eta_{CCS}$ (4)

CO_2 capture efficiency: $\eta_{cap} = \dfrac{CO_2\ captured}{CO_2\ produced}$ (5)

CO_2 avoidance: $\eta_{avoid} = \dfrac{E_{ref} - E_{CCS}}{E_{ref}}$ (6)

Specific primary energy consumption for CO_2 avoided: SPECCA

$= \dfrac{\left(\frac{1}{\eta_{CCS}} - \frac{1}{\eta_{ref}}\right)}{E_{ref} - E_{CCS}} \cdot 3600$ (7)

where η is the efficiency (%), $\dot{W}$ is the net power produced (kW), $\dot{m}$ is the fuel mass flow (kg/s), LHV is the fuel lower heating value (kJ/kg), and E is the emission intensity (kg/kWh). The subscript *ref* stands for reference plant and *CCS* stands for the different CO_2 capture plants considered.

Table 2
Plant specifications and main assumptions.

Unit	Specification
Natural gas (vol. %)	CH_4 – 89%; C_2H_6 – 7%; C_3H_8 – 1%; C_4H_{10} – 0.11%; CO_2 – 2%; N_2 – 0.89% (70 bar and 15 °C)
Air composition (vol. %)	N_2 – 77.38%; O_2 – 20.76%; CO_2 – 0.03% H_2O – 0.91%; Ar – 0.92% (1.013 bar and 9 °C)
Filter pressure loss (Pa)	750
Hydrogen supply, °C/bar	15/35
LHV - NG/H_2, (kJ/kg)	46502/119800
Combustor pressure drop	3%
ICR pressure drop	0.5 bar
Air compressor polytropic efficiency	92%
Gas/CO_2 expander polytropic efficiency	92/85%
Compressors isentropic efficiency	85%
Mechanical efficiency	98%
Steam cycle (HRSG)	
Steam turbine system	Condensing reheat steam turbine
Reheat temperature, °C	600
HP/IP/LP steam pressure, bar	185/43/6
HP/IP/LP steam temperature, °C	600/320/300
Pinch temperature/Approach temperature, °C	9/10
Condenser pressure, bar	0.04
Cooling system	Water cooling with natural draft cooling tower
Water pump efficiency	70%
CO_2 compression	
Compression stages	3
Final CO_2 condition, °C/bar	30/110
Compressor stages isentropic efficiency	80/80/75%
CO_2 pump efficiency	75%

2.3. Economic analysis and assumptions

This section describes the adopted cost estimation methodology for the capital costs and the operation and maintenance (O&M) costs. The O&M estimation methodology is based on the guidelines for the techno-economic assessment of power plants by the National Energy Technology Laboratory (NETL) [39]. For the gas turbine, a specific cost of $ 219/kW was assumed based on the guidelines from Ref. [32]. An additional 2.5% cost increase was considered to account for transportation. The equipment modeled in Aspen Plus were sized according to the simulation data and the equipment costs were estimated based on the year 2017 US dollars. However, the reactor costs were estimated using the methodology from Turton et al. [40]. In the ICR-CC case, a total of 20 reactor units were assumed with a diameter of 3.45 m and a height of 6.9 m. This large number of reactors was required because of the relatively low fluidization velocity of 1 m/s that was assumed. Detailed reactor simulations [30] showed that the ICR works well under these operating conditions with low particle elutriation. However, cases with higher fluidization velocities are also considered to reduce the number of reactors required in a sensitivity analysis presented later. Higher fluidization velocities will reduce reactor costs, but will also require more elaborate gas-particle separation systems to prevent excessive elutriation of particles.

Each reactor was assumed to consist of two process vessels: the ICR body manufactured from an expensive Ni-alloy for carrying the thermal and corrosive loads, and a thick outer pressure shell manufactured from carbon steel for carrying the pressure load. A 40 cm layer of insulation material separates the ICR body and the outer shell. In the base case, the cost of the Ni-alloy vessel representing the ICR body was tripled to account for the more complex internal structure of the ICR as well as any gas-particle separation equipment that may be required. This is a crude assumption and will also be varied in a sensitivity analysis next to the fluidization velocity.

The cost of the initial OC loading was also included in the capital costs, using a cost of $15/kg [41] and was assumed to occupy 20% of the reactor volume. The reactivity and the lifetime are critical to the overall OC costs [42]. Given the high thermal and attrition loads, the OC was assumed to be replaced every 2 years. Following Turton et al. [40], the auxiliaries for the reactor is assumed to be 50% of the vessel, pressure shell and insulation costs under standard conditions (carbon steel at atmospheric pressure) whereas the contingency is assumed to be 18% of the total reactor cost.

Fig. 5 shows the reactor cost breakdown in the base case for all the ICR plant configurations. It is to be noted that the reactor cost is estimated based on the air flowrate in the AS. Thus, the reactor cost is more for the ICR-CC base case as the airflow rate was higher than that in other cases (823 kg/s relative to 756–771 kg/s). An additional cost benefit is achieved in the cases with added firing because of about 5 bar higher operating pressure. This allows for smaller reactors to be used when the fluidization velocity is fixed at 1 m/s. In all the cases, the reactor vessel accounts for the bulk of the overall costs due to the complexity in the design and manufacture. The pressure shell cost is also high, followed by the contingencies and the OC, while the auxiliaries and insulation material costs are small.

The cost of the equipment involved in the steam cycle is obtained directly from the PEACE component in Thermoflex. However, the cooling tower costs are calculated using equation (8). The scaling exponent for sizing the cooling tower is considered as 0.71 and is acquired from the literature [43]. The installed cost data of all the equipment is obtained converted to 2019 dollars using the chemical engineering plant cost index (CEPCI) shown in equation (9) [44]. The annual averaged CEPCI for the years 2017 and 2019 is 567.5 and 616.2, respectively.

$$\text{Cost of equipment A} = (\text{Cost of equipment B}) \times \left(\frac{\text{Capacity of A}}{\text{Capacity of B}} \right)^{\text{exponent}}$$

$$(8)$$

$$\text{Present cost} = \text{Original cost} \times \left(\frac{\text{CEPCI at present}}{\text{CEPCI at time of original cost}} \right)$$

$$(9)$$

As mentioned earlier, the capital cost estimation is performed based on the Thermoflex assumptions [34]. The methodology consists of seven elements: direct material costs (DMC), construction costs, engineering, procurement and construction costs (EPC), contingencies, startup costs, other costs, and total plant cost (TPC) as shown in Table 3. The DMC is comprised of only the equipment costs while the construction costs include civil, mechanical, electrical assembly, wiring, building, and structures as needed for the installation of the equipment. The startup cost comprises of costs associated with registrations, legalities, employee training, and promotional activities. The other costs include temporary facilities, license fees, and other minor costs. The calculation of the cost elements is based on the assumptions given in Table 3 and is taken from Thermoflex [34].

The assumptions adopted for the O&M costs are listed in Table 3. For fixed O&M costs, the labor requirement is calculated using the guidelines given by Peters and Timmerhaus [44]. For the NGCC plants with and without capture, the operating labor requirements are 13 and 11 workers, respectively. For the ICR-CC, the ICR-NG and the ICR-H$_2$ cases, the number of workers required is 14, while 13 workers are required for the ICR-H$_2$-2P case. An average labor cost of $45/hr is assumed for power plant operators and maintenance workers in Europe. The price for natural gas is taken as $8.4/GJ [45] and the price of H$_2$ is assumed to be $15.5/GJ, which can be expected from an advanced hydrogen production process with CO$_2$ capture such as membrane-assisted autothermal reforming [41]. A sensitivity study on these fuel prices is presented later. The prices of the process water and the cooling water considered are $2/m^3 and $0.35/m^3, respectively [41]. The cost of CO$_2$ transport and storage was assumed $12/ton-CO$_2$ [46]. The sensitivity of the LCOE to different CO$_2$ prices is presented later.

The performance indicators for the economic assessment are the levelized cost of electricity (LCOE) and the cost of CO$_2$ avoidance. The LCOE is calculated based on the discounted cash flow analysis with a discount rate of 8% as given in Ref. [47]. Eqs. (10) and (11) are used to calculate LCOE and the cost of CO$_2$ avoidance, respectively.
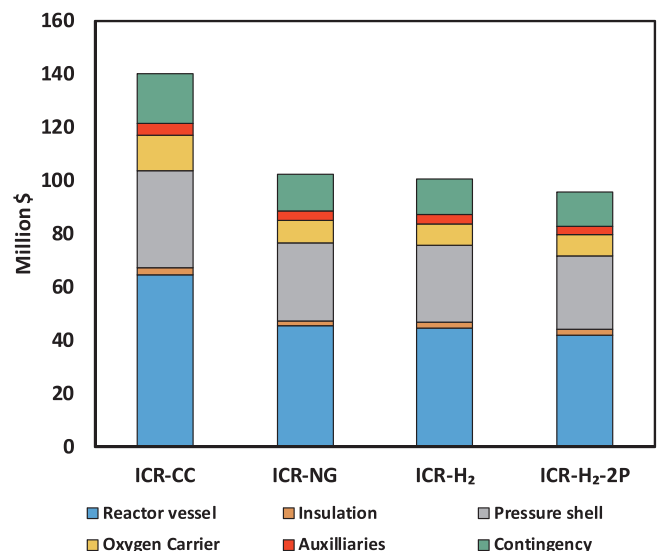

Fig. 5. Breakdown of reactor cost.

Table 3
Capital costs and O&M costs assumptions.

Capital cost estimation	
Base year	2019
Direct material cost (DMC)	Equipment cost
Construction	
Civil	16% of DMC
Mechanical	17% of DMC
Electrical assembly and wiring	4% of DMC
Buildings and structures	8% of DMC
Other costs	8% of DMC
Engineering, procurement and construction (EPC)	16% of DMC
Contingencies	16% of DMC
Start-up	6% of DMC
Total plant cost (TPC)	191%
Operation and Maintenance cost estimation	
Capacity factor	85%
Plant lifetime	30 years
Total fixed operating cost	
Labor rate (base)	45 $/hr
Labor per shift	11–14
Operating labor burden	30% of base
Labor overhead charge rate	25% of labor
Maintenance labor	25% of operating labor
Property taxes and insurance	1.5% of TPC
Total variable operating cost	
Natural gas	8.4 $/GJ
Nickel oxide	15 $/kg
OC replacement period	2 years
Process water	2 $/m^3
CO_2 transport and storage costs	12 $/ton CO_2
Emission tax (CO_2 tax)	27 $/ton CO_2

$$LCOE \ (\$/MWh) = \frac{\sum_{t=1}^{n} \frac{I_t + M_t + F_t}{(1+r)^t}}{\sum_{t=1}^{n} \frac{E_t}{(1+r)^t}} \qquad (10)$$

$$CO_2 \ avoidance \ cost \ (\$/ton) = \frac{(LCOE)_{CCS} - (LCOE)_{ref}}{E_{ref} - E_{CCS}} \qquad (11)$$

where I_t is the investment expenditures in year t (including financing), M_t is the O&M expenditures in year t, F_t is the fuel expenditure in year t, E_t is the electricity generation in year t, r is the discount rate and n is the plant life.

3. Results and discussions

Results are presented in two sections: technical and economic. In the technical analysis, the plant performance is presented in terms of net electrical efficiency, efficiency penalty, CO_2 capture efficiency, and CO_2 avoidance. Subsequently, the results of the economic analysis in terms of LCOE and CO_2 avoidance costs are also presented. In addition, the sensitivity of these parameters to the changes in key economic parameters such as fuel costs, CO_2 tax, capacity factor and reactor cost assumptions are also presented.

3.1. Technical assessment

The results of the technical performance indicators are presented in Fig. 6. The net electrical efficiency of the NGCC reference plant obtained is 62.1%. Conventional post-combustion CO_2 capture imposes an efficiency penalty of 8.1%-points, which is within the range (7.6–8.4%-points) reported in the literature [6,31]. Table 4 presents the power consumption and production of the major equipment as a percentage of LHV input. The power consumption of the auxiliaries including pumps is very small (~1.1%). The gas turbine produces the bulk of the net power, 43% of LHV input, followed by the steam turbines at 20.2% of LHV input. The stream information on key plant locations shown in Fig. 2 is presented in Table 5. It is to be noted that the COT of NGCC

plant is 1647.8 °C (stream 5), which results in the gas turbine outlet temperature (TOT) of 641 °C (stream 6). At these conditions, sufficient heat is available to produce a significant amount of superheated steam, which is evident by the power generated by the steam turbine assembly (20.2% of LHV). For the NGCC-PCC case, auxiliary consumption increases to 4% of LHV input due to compression and pumping in the CO_2 capture process. Due to the steam requirement in the stripper column, the steam turbine power output reduces to 15% of LHV input. Thus, an overall drop of 8.1%-points in the net electrical efficiency is observed. As mentioned earlier, a CO_2 capture efficiency of 90% is assumed that results in CO_2 avoidance of 88.5%. Hence, the SPECCA amounts to 2.95 MJ/kg.

The net electrical efficiency of the ICR-CC plant obtained is 50.7% – an efficiency penalty of 11.4%-points relative to the reference NGCC plant. On the other hand, when compared to the NGCC-PCC case, the efficiency penalty observed is 3.3%-points and the SPECCA is 1.24 MJ/kg higher. Thus, even though CLC imposes almost no direct energy penalty related to CO_2 capture, the indirect energy penalty caused by the maximum temperature limitation of the reactor makes the overall plant significantly less efficient than a conventional NGCC plant with post-combustion CO_2 capture.

An additional drawback of the ICR-CC plant is the much larger air/fuel ratio required to maintain 1150 °C in the reactor, relative to the other plants that heat the air to a temperature of 1647.8 °C. This will require considerably larger compressors and turbines per unit LHV input. In addition, this larger gas turbine will need to be custom designed for the ICR-CC plant. As a result of the low TIT, the net power generation from the gas turbine is only 32.2% of LHV input, while the steam turbine output is only 15.5% of LHV due to a low TOT of 488 °C. The power produced by the CO_2 expander is 5.9% of LHV input, which offsets the power consumed in compressing CO_2 to transport and storage conditions. The energy penalty for CO_2 compression is just 2.2% of LHV input, which is lower than that required for capture and compression in the NGCC-PCC plant with MEA-based capture systems. Based on the CFD analysis [30], the CO_2 capture efficiency is maintained at 95% that translates into CO_2 avoidance of 93.9% with respect to the reference plant.

Fig. 7 presents the performance results of the ICR cases with an added combustor. The power generation and consumption results of the cases ICR-H$_2$, ICR-NG and ICR-H$_2$-2P are presented in Table 3, while Table 6 presents the stream information for the ICR-H$_2$ case.

The net electrical efficiency obtained for the ICR-NG and the ICR-H$_2$ cases are almost identical at 60.7%, resulting in an energy penalty of 1.4%-points. Due to higher specific emissions, the ICR-NG case has a higher SPECCA of 0.77 MJ/kg relative to 0.41 MJ/kg in the ICR-H$_2$ case. This is a substantial improvement when compared to the penalty
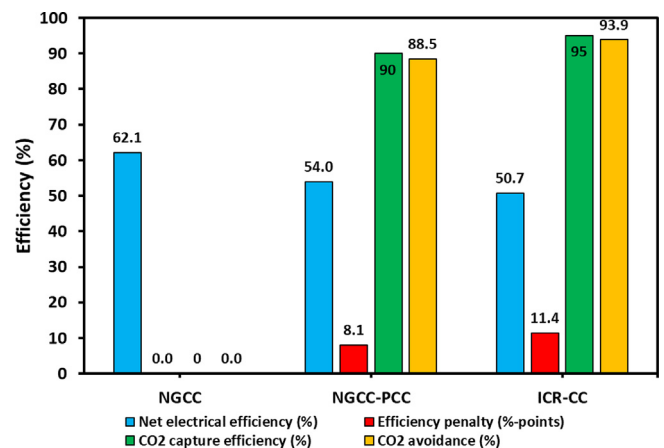

Fig. 6. Performance of the ICR-CC configuration compared to the benchmark NGCC plants with and without CO_2 capture.

Table 4
Power generation and consumption based on fuel input for all power plant configurations.

	NGCC	NGCC-PCC	ICR-CC	ICR-NG	ICR-H₂	ICR- H₂-2P
Fuel input (MW)	1209.3	1209.3	697.5	1134.8	1147.1	1151.3
Auxiliary (% LHV)	−1.1%	−1.0%	−0.7%	−1.1%	−1.1%	−1.1%
CO_2 compressors (% LHV)	0.0%	−3.0%	−2.2%	−1.2%	−1.2%	−0.4%
Gas turbine (% LHV)	43.0%	43.0%	32.2%	40.2%	40.6%	43.2%
CO_2 expander (% LHV)	0.0%	0.0%	5.9%	3.4%	3.4%	0%
Steam turbine (% LHV)	20.2%	15.0%	15.5%	19.5%	19.1%	19.8%
Net power (MW)	750.94	653.14	353.52	688.57	696.39	708.05
Net electrical efficiency (%)	62.10	54.01	50.68	60.68	60.71	61.50
Specific emissions (kg/MWh)	332.23	38.20	20.25	157.19	9.47	9.29
SPECCA (MJ/kg)		2.95	4.19	0.77	0.41	0.17

and SPECCA associated with CO_2 capture using MEA-based systems (~8.1%-points and 2.95 MJ/kg) [5]. In the ICR-H₂ case, the gas turbine generation of 40.6% of LHV input is slightly higher than the 40.2% in the ICR-NG, which is compensated by slightly lower generation from the steam turbine assembly (19.1% of LHV input relative to 19.5%). This is due to an 8 K higher TOT in the ICR-NG case than the ICR-H₂ case. The power produced by the CO_2 expander and consumption in CO_2 compression is the same in both cases.

Although the ICR has a CO_2 capture efficiency of 95%, Fig. 7 shows that the CO_2 capture efficiency for the ICR-NG case is only 53%. The reduction in capture efficiency is due to the CO_2 produced in the NG-fired added combustor. This CO_2 was not captured and was released into the atmosphere. Therefore, the CO_2 avoidance for the ICR-NG and the ICR-H₂ cases are 52.4% and 94.9%, respectively.

Table 4 also shows the power generated and consumed the ICR-H₂-2P case where the H₂ fuel was diluted with efficiently generated steam and preheated to 800 °C before injecting into the combustor (Stream 10 in Table 7). In essence, this plant configuration allows the steam that is expanded in the CO_2 turbine in the other ICR cases to instead be expanded in the main gas turbine, thus increasing the volume flow through the main expander to achieve power production closer to the design capacity of the turbine. Specifically, the gross gas turbine output is 520 MW in the conventional NGCC plant, 456 MW in the ICR-NG case, 466 MW in the ICR-H₂ case, and 497 MW in the ICR-H₂-2P case, illustrating the ability of the ICR-H₂-2P configuration to better utilize the gas turbine. Table 4 shows that the combined power output of the gas and steam turbines is similar to the ICR-NG and ICR-H₂ cases, with a slight shift to power generation by the steam turbines due to the higher flow rate of flue gases available for heat recovery. Since the CO_2 expander is not required in this case, the CO_2 stream is not expanded to atmospheric pressure before compression, resulting in significantly lower CO_2 compression power consumption of 0.4% of LHV input relative to 1.2% for the other added firing ICR cases. This saving increases the net electrical efficiency to 61.5% with an efficiency penalty of only 0.6%-points and a negligible SPECCA of 0.17 MJ/kg. The CO_2 capture efficiency and CO_2 avoidance are similar to that of the ICR-H₂ case.

The results presented in Fig. 7 for the ICR-H₂-2P case is for the ideal
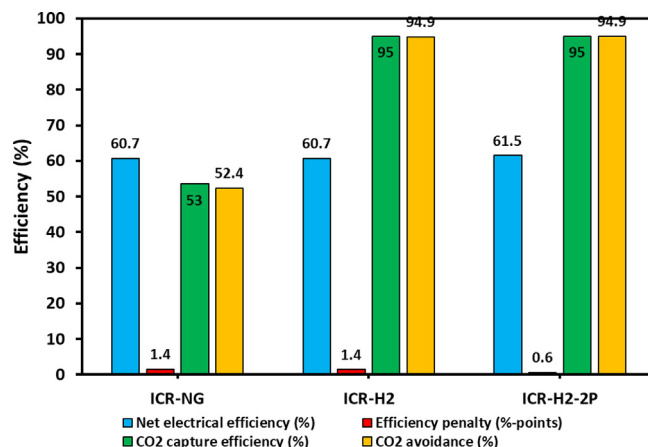

Fig. 7. Performance comparison of ICR cases with additional combustors.

case of 100% efficiency and 100% capture in the H₂ production plant supplying hydrogen to the added combustor. However, some losses are always involved in hydrogen production. For a more realistic assessment, the three different scenarios outlined in a previous study by the authors [31] is also briefly assessed here: a) Steam-methane reforming with conventional CO_2 capture (70% efficiency and 80% capture); b) Advanced method such as membrane-assisted chemical looping reforming [48] (80% efficiency and 90% capture); and c) Advanced method with high degree of process integration (90% efficiency and 100% capture). The results obtained after considering the aforementioned three cases for the H₂ production plant are presented in Fig. 8. It can be observed that the conventional H₂ source reduces the net electrical efficiency and CO_2 capture efficiency to 51.68% and 86.99%, respectively, which is lower to the NGCC case with MEA-based CO_2 capture (NGCC-PCC). The advanced H₂ production process (b) performs slightly better than the NGCC-PCC case, but only the case with high process integration (c) can outperform the NGCC-PCC case.

As an example of a process integration corresponding to option (c),

Table 5
Stream data for the NGCC plant.

St.	T	P	Mass flow	Mole composition (%)						
	°C	bar	kg/s	CH_4	C_{2+}	N_2	O_2	CO_2	H_2O	Ar
1	9.0	1.01	947.6	0	0	77.38	20.76	0.03	0.91	0.922
2	455.8	23.74	739.3	0	0	77.38	20.76	0.03	0.91	0.922
3	10.0	35.00	26.0	89.00	8.11	0.89	0	2	0	0
4	220.0	35.00	26.0	89.00	8.11	0.89	0	2	0	0
5	1647.8	23.02	765.3	0	0	73.81	10.67	4.73	9.79	0.79
6	641.0	1.04	973.6	0	0	74.02	11.10	4.59	9.42	0.88
7	89.6	1.02	973.6	0	0	74.02	11.10	4.59	9.42	0.88
8	29.5	3.91	165.3	0	0	0	0	0	100	0
9	29.0	0.04	165.2	0	0	0	0	0	100	0

Table 6
Stream data of ICR combined cycle plant with H_2-fired combustor (ICR-H_2).

St.	T	P	Mass flow	Mole composition (%)							
	°C	bar	kg/s	CH$_4$	C$_{2+}$	N$_2$	O$_2$	CO$_2$	H$_2$O	Ar	H$_2$
1	9.0	1.01	947.6	0	0	77.38	20.76	0.03	0.91	0.92	0
2	448	22.83	767.4	0	0	77.38	20.76	0.03	0.91	0.92	0
3	1160	22.33	718.5	0	0	81.92	15.62	0.20	1.38	0.88	0
4	1648	21.66	722.7	0	0	78.65	11.01	0.19	9.31	0.84	0
5	633	1.05	904.4	0	0	78.38	12.91	0.16	7.62	0.93	0
6	91	1.02	904.4	0	0	78.38	12.91	0.16	7.62	0.93	0
7	10	70	13.8	89	8.11	0.89	0.00	2	0	0	0
8	439	18.44	13.8	89	8.11	0.89	0.00	2	0	0	0
9	15	35	4.2	0	0	0	0	0	0	0	100
10	289	35	4.2	0	0	0	0	0	0	0	100
11	869	17.54	62.6	0	0	1.72	0	34.15	64.12	0.02	0
12	300	1.03	62.6	0	0	1.72	0	34.15	64.12	0.02	0
13	110	1.02	62.6	0	0	1.72	0	34.15	64.12	0.02	0
14	30	110	35.9	0	0	4.78	0	94.97	0.21	0.04	0
15	29	3.91	149.7	0	0	0	0	0	100	0	0
16	29	0.04	149.6	0	0	0	0	0	100	0	0

the exhaust gases from the CLC FS can be used as a source of steam in a membrane-assisted chemical looping reforming (MA-CLR) process [48] for efficient hydrogen production. In this case, a similar two-phase flow heat exchanger as presented in this case (ICR-H_2-2P) can be used to recover the condensation enthalpy in the CLC FS outlet gas to efficiently generate a stream of natural gas and steam for the MA-CLR plant. As shown in previous work [49], the need to raise steam is the primary energy penalty in pre-combustion CO_2 capture plants based on chemical looping technology, and this penalty can largely be avoided by capitalizing on the pressurized steam from natural gas combustion that is captured together with the CO_2 in the CLC process. Future work will investigate the performance of such an integrated CLC and MA-CLR plant where MA-CLR provides H_2 for added firing to make CLC power production more efficient and CLC supplies the captured steam from natural gas combustion to improve the hydrogen production efficiency of MA-CLR.

Finally, it should be mentioned that the ICR configuration with added firing could be advantageous for flexible operation. During part-load operation, the TIT of the gas turbine reduces, requiring less added firing above the maximum achievable temperature in the ICR. For example, a combined cycle power plant with an HA-class turbine operating at 48% load (40% gas turbine load) will have a reduction in TIT of 143 °C [50] – about 30% of the temperature increase over the ICR temperature facilitated by the added combustor. Thus, a smaller fraction of fuel will need to be combusted in the added combustor, increasing the CO_2 capture efficiency of the ICR-NG case and lowering the
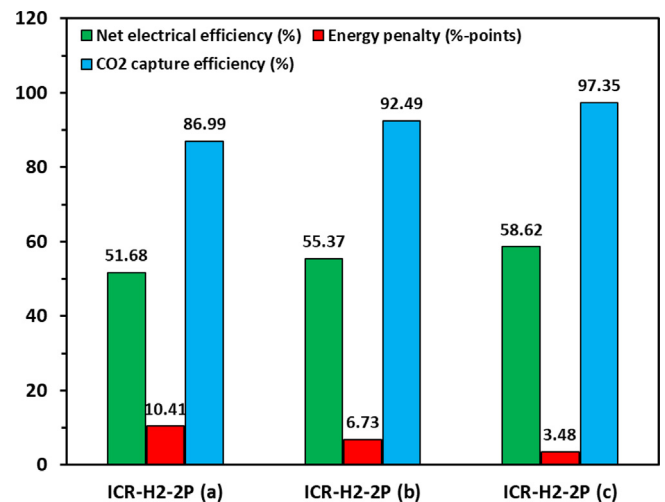

Fig. 8. Effect of H_2 source on the plant performance.

fuel costs from combusting costly H_2 in the ICR-H_2 case. In addition, the MILD combustion conditions in the added combustor could help reduce NOx emissions related to the part-load operation.

Flexible operation of the ICR unit should not introduce serious technical challenges. Part-load operation reduces the required air and fuel flow rates but also reduces the required pressure ratio. For

Table 7
Stream data of ICR combined cycle plant with saturated H_2-fired combustor (ICR-H_2-2P).

St.	T	P	Mass flow	Mole composition (%)							
	°C	bar	kg/s	CH$_4$	C$_{2+}$	N$_2$	O$_2$	CO$_2$	H$_2$O	Ar	H$_2$
1	9.0	1.01	947.6	0	0	77.38	20.76	0.03	0.91	0.92	0
2	455	23.61	756.1	0	0	77.38	20.76	0.03	0.91	0.92	0
3	1160	23.11	707.4	0	0	81.98	15.56	0.20	1.38	0.88	0
4	1648	22.42	731.5	0	0	75.40	10.38	0.18	13.23	0.81	0
5	633	1.05	924.9	0	0	75.70	12.45	0.15	10.80	0.90	0
6	91	1.02	924.9	0	0	75.70	12.45	0.15	10.80	0.90	0
7	30	18.44	13.8	89	8.11	0.89	0	2	0	0	0
8	15	35	4.3	0	0	0	0	0	0	0	100
9	15	1.01	19.8	0	0	0	0	0	100	0	0
10	800	34.65	24.1	0	0	0	0	0	34.24	0	65.76
11	846	17.54	62.4	0	0	1.64	0	34.18	64.17	0.01	0
12	30	110	35.8	0	0	4.57	0	95.24	0.14	0.04	0
13	29	3.91	156.0	0	0	0	0	0	100	0	0
14	29	0.04	155.9	0	0	0	0	0	100	0	0

example, the same 40% operating point of the HA-class turbine mentioned above reduces the flow rate through the gas turbine by 44% and the pressure by 40% [50]. Hence, the fluidization velocity in the ICR unit will remain largely unchanged, leading to similar hydrodynamic conditions in the reactor.

3.2. Economic assessment

The economic assessment will be presented in two parts: an evaluation of the base case results and an analysis of the sensitivity of the results to variation of parameters involving high uncertainty.

3.2.1. Base case results

Fig. 9 shows the main results of the economic assessment. It is evident that fuel accounts for the largest component of the levelized costs at the relatively high European fuel prices assumed in this study. Capital costs and fixed operating and maintenance (O&M) costs represent the next most important cost components. Variable O&M is small in all the plants, although it is larger in the plants involving ICR due to the OC replacement costs. CO_2 transport and storage (T&S) costs are also significant in all CCS plants, although it is noticeably lower in the ICR-NG case that only avoids 52.4% of CO_2.

When considering CO_2 avoidance costs (CAC), the benchmark NGCC-PCC case can avoid CO_2 for $93.8/ton, which agrees well with values reported in the review by Rubin et al. [51]. The ICR-CC case shows $23.5/ton higher CAC than the NGCC-PCC reference, illustrating the large disadvantage created by the maximum temperature limitation of the CLC process when implemented into combined cycle power plants. The additional combustor added in the ICR-NG plant addresses this fundamental shortcoming, reducing the CAC to $60.3/ton. This value may appear relatively high given that the LCOE of the ICR-NG case is only $10.4/MWh higher than the NGCC reference plant, but the low CO_2 avoidance of the ICR-NG plant increases the CAC. When CO_2 emissions from the added combustor are avoided by combusting clean H_2 instead of NG in the ICR-H_2 case, CO_2 avoidance costs increase to the level of the NGCC-PCC reference case. Fig. 9 shows that the capital cost of the ICR-H_2 case is much lower than that of the NGCC-PCC case, but this advantage is canceled out by the high costs of hydrogen. In the base case, NG costs $8.4/GJ and H_2 costs $15.5/GJ. Since the ICR-$H_2$ plant must consume 44% of its LHV fuel input as an expensive H_2, the impact on total fuel costs is large. Thus, even though the CO_2 avoidance of the ICR-H_2 case is much larger than that of the ICR-NG case, its CAC is considerably higher at $96.3/ton. Finally, the ICR-H_2-2P case shows a slight improvement in CAC to $90.3/ton due to its higher efficiency and slightly lower capital costs.

Fig. 10 shows the capital cost breakdown of the different plants evaluated in this study. The NGCC-PCC plant is the most expensive due to the high cost of the CO_2 capture unit (which includes CO_2 compression). The specific capital costs ($/kW) of the power plant components in the NGCC-PCC case also increase relative to the NGCC case due to the energy penalty. These power plant components become even more expensive in the ICR-CC case, which imposes a large energy penalty and imposes higher gas turbine costs due to the large air flowrate required per unit of power output. The components related to CO_2 capture (the ICR, CO_2 expander, CO_2 compressors, and heat exchangers) are 28% cheaper than the CO_2 capture plant in the NGCC-PCC case. This is conceivable given the much smaller equipment size facilitated by pressurized operation and a highly active oxygen carrier, as well as the lack of internal heat transfer surfaces, packing material and steam cycle integration.

The ICR cases with added firing result in a strong reduction in the reactor cost. Relative to the ICR-CC case, the cost of the ICR unit in the ICR-NG case reduces by 63%. This is partly due to the lower absolute capital cost of the reactor shown in Fig. 5, but primarily due to the ICR-NG plant producing about twice as much electricity per unit of air flowing through the ICR than the ICR-CC case. Due to the added firing, each unit of air accumulates much more thermal energy which is then converted to electrical energy at a higher efficiency. The capital cost of the ICR-H_2 case is almost identical to that of the ICR-NG case. In the ICR-H_2-2P case, the cost of the large 2-phase flow heat exchanger is only marginally less than the cost of the CO_2 expander and the additional CO_2 compression stages. This, in combination with the slightly smaller ICR unit (Fig. 5) and slightly better utilization of the gas turbine, achieves a 4.1% capital cost reduction relative to the ICR-H_2 case.

3.2.2. Sensitivity analysis

This section will compare the performance of the different CO_2 capture plants over several important variables including CO_2 price, capacity factor, fuel prices, and reactor cost uncertainties. The effect of changes in CO_2 price is illustrated in Fig. 11. The gradients of the different lines are indicative of the CO_2 intensity of the different plants, and points of intersection with the NGCC reference plant indicates the CO_2 avoidance cost. Fig. 11 shows that the ICR-NG case only becomes more expensive than the NGCC-PCC case at a CO_2 price of $140/ton. At this point, the plant could be retrofitted to fire the added combustor with H_2 instead of NG.

Fuel costs also have a large effect on the economic performance of the different plants. Natural gas prices are known to vary widely over
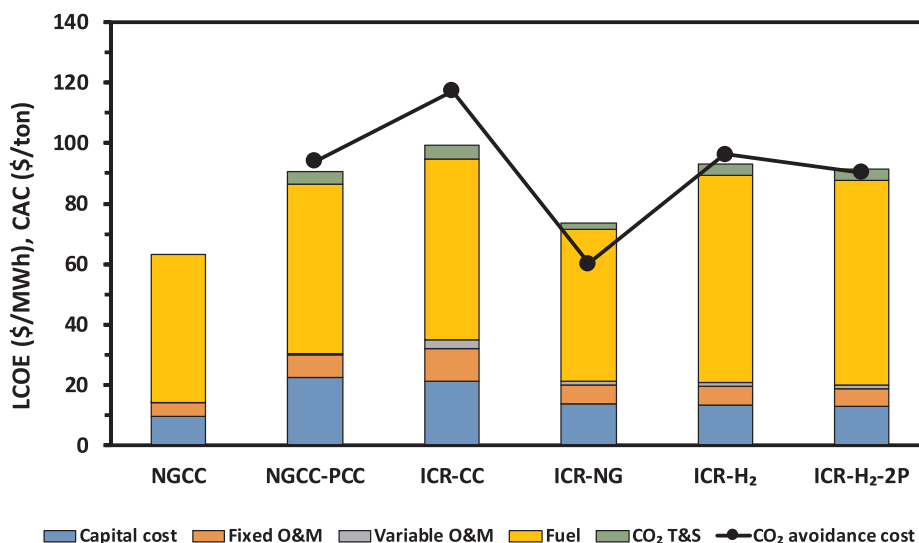
Fig. 9. Levelized cost of electricity (LCOE) and CO_2 avoidance costs (CAC) of the six plants evaluated in this study.
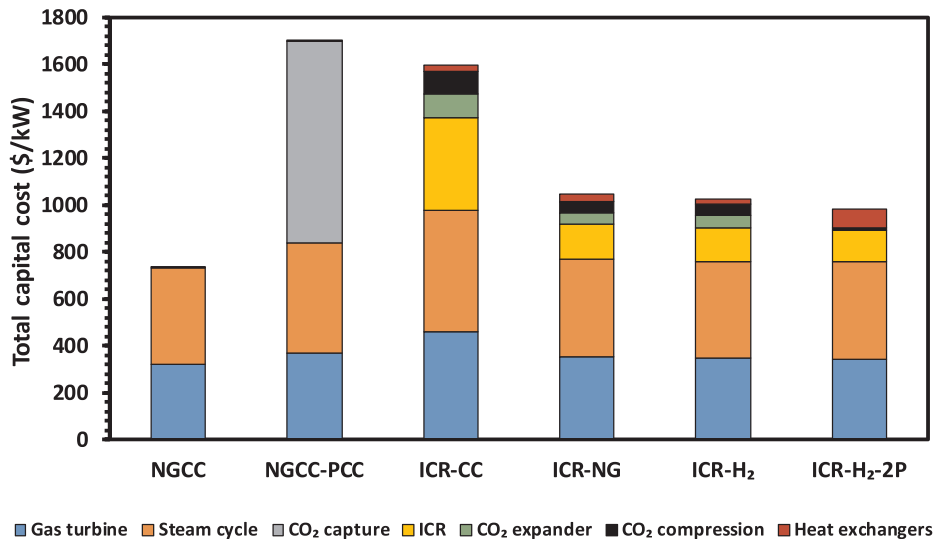
Fig. 10. Breakdown of the capital costs of the six different plants evaluated in this study.
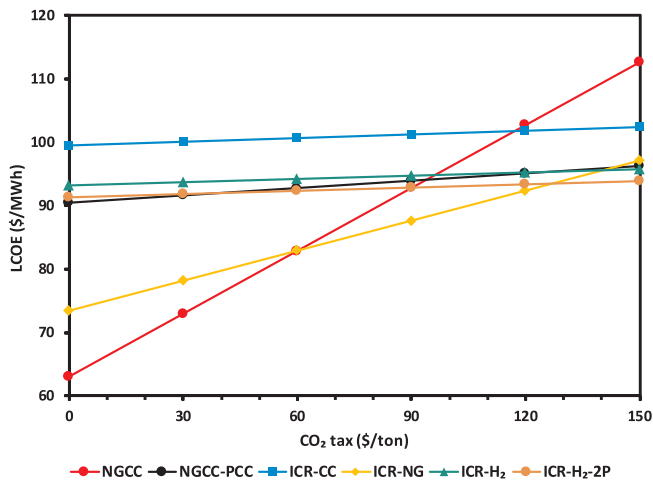
Fig. 11. Sensitivity of the LCOE to variations in the CO_2 price.

$P_{H_2} = 5 + P_{NG}/0.8$, which is representative of the membrane-assisted autothermal reforming process [41].

Fig. 12 shows the expected behavior that the NG price has a larger effect on the plants with the lowest efficiency. Therefore, the CO_2 avoidance cost of the ICR-CC plant is most affected, whereas the ICR-NG plant is least affected. The ICR-H_2 and ICR-H_2-2P plants are more sensitive than the ICR-NG plant due to the assumption that NG can be converted to H_2 with an efficiency of 80%. However, despite this assumed loss during H_2 production, these plants are still slightly less sensitive than the NGCC-PCC plant. Naturally, the ICR-H_2 and ICR-H_2-2P plants are highly sensitive to the H_2 price. This is illustrated in Fig. 12 with a NG price of \$8.4/GJ. A highly integrated advanced hydrogen production process can conceivably reduce the H_2 price significantly below the \$15.5/GJ level used in the base case, resulting in substantial savings relative to the NGCC-PCC reference case.

The capacity factor chosen for the base case (85%) is typical of power plant economic assessments reported in the literature. However, NGCC plants are mostly deployed as load-following plants operating at lower capacity factors and this trend is set to continue as more variable renewable energy is brought online. To investigate this effect, two sensitivity analyses to the capacity factor are completed, changing the way in which the capacity factor influences the economics of the cases with added hydrogen firing. In the first case, it is assumed that the
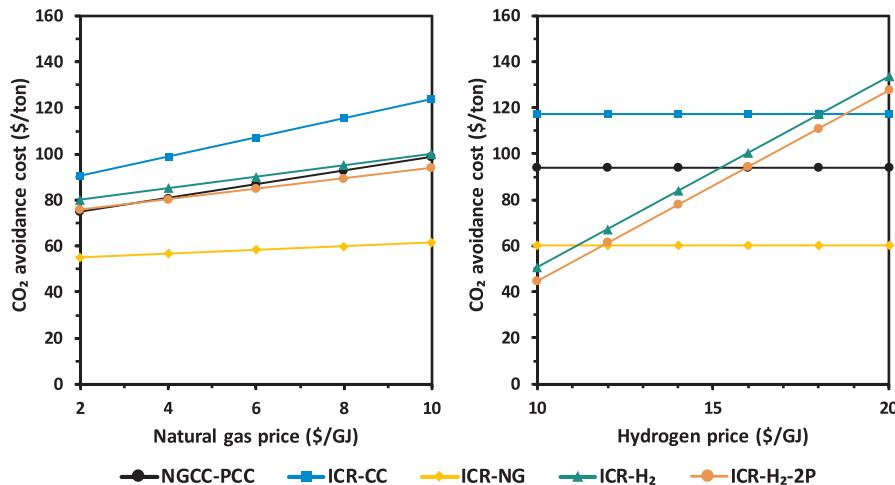
time and between different world regions. Clean hydrogen prices are highly dependent on the hydrogen production process and, if a reforming process is used, the natural gas price. In the NG price sensitivity study presented here, the hydrogen price is assumed to be

Fig. 12. Sensitivity of the CO_2 avoidance cost to NG and H_2 prices.

reforming process supplying hydrogen for added firing must also reduce its capacity factor with that of the power plant. This is done by adjusting the hydrogen price as follows: $P_{H_2} = 5 \cdot 0.85/CF + 1.05$, accounting for the fact that a lower capacity factor (CF) will increase the magnitude of the fixed cost portion of the levelized cost of hydrogen. In the second case, the hydrogen price was assumed to remain at $15.5/GJ on the assumption that the hydrogen plant can continue operating at a high capacity factor, even as the power plant is operated at a lower capacity factor to follow load. This case will significantly improve economic performance at lower capacity factors, but it requires an established hydrogen market to absorb the pure hydrogen produced during times when it is not needed by the power plant. Such flexible power and hydrogen production was shown to be highly beneficial to future energy systems with high shares of variable renewables [52].

The capacity factor was varied in the range 30–90% and the results for CAC are presented in Fig. 13. As expected, reducing the capacity factor increases the CAC significantly for all cases. This is due to the decrease in the number of annual operating hours which increases the contribution of the capital and fixed operating costs towards the CAC. The plants with the highest fixed costs (NGCC-PCC and ICR-CC) are most affected by a lower capacity factor. When the hydrogen production process is assumed to also ramp down with the power plant (Fig. 13, left), the sensitivity of the ICR-H$_2$ and ICR-H$_2$-2P cases show a similarly large sensitivity. However, these cases perform much better at lower capacity factors when the hydrogen production process is allowed to continue operating at a high capacity factor (Fig. 13, right). This is due to the relatively low capital costs of the cases with added firing (Fig. 10). The ICR-NG case also has relatively low capital costs, but this plant still experiences significant increases in CAC at lower capacity factors due to its lower CO$_2$ avoidance. It should also be mentioned that the low capacity factor performance of the cases with added firing could be significantly better than indicated in Fig. 13 due to the reduction in the amount of added firing required under part-load operation. As discussed in the technical assessment, the reduced TIT under part-load operation will increase the CO$_2$ avoidance of the ICR-NG case and reduce the large H$_2$ fuel costs in the ICR-H$_2$ and ICR-H$_2$-2P cases.

As mentioned in the methodology, there is substantial uncertainty with respect to the ICR capital cost estimation. Fig. 14 shows a moderate influence of the assumptions used in the ICR cost assessment on the CO$_2$ avoidance cost. An increase in the fluidization velocity above the base case assumption of 1 m/s will reduce the number of reactors required, thereby reducing the total reactor cost. For example, increasing the fluidization velocity in the ICR-NG case from 1 m/s to 2 m/

s will reduce the number of reactors required from 20 to 10, thereby lowering the reactor cost from $102 million to $51 million and reducing the CO$_2$ avoidance cost from $60.3/ton to $53.7/ton. This is a significant cost reduction but will be offset to a certain degree by more expensive gas-particle separation equipment required to prevent excessive particle elutriation. Fig. 14 shows that an increase in the reactor cost adjustment factor accounting for added costs over that of a simple process vessel only has a moderate effect. In the ICR-NG case, an increase of this factor from the base value of 3 to 5 will increase CO$_2$ avoidance cost from $60.3/ton to $64.1/ton. These results show that the uncertainty involved in the reactor cost estimation will not have a decisive influence on the conclusions drawn from this study.

4. Conclusions

The application of CLC to power production from natural gas faces a fundamental problem: the maximum reactor temperature will always be far below the continuously increasing firing temperatures of modern gas turbines. This creates a large indirect energy penalty that renders the CLC concept economically uncompetitive relative to a conventional NGCC plant with post-combustion CO$_2$ capture. To overcome this limitation, an added combustor after the CLC unit is needed. This allows the CLC plant to utilize current state-of-the-art gas turbines and greatly reduce the energy penalty.

Results from the present study show that added natural gas firing reduces the energy penalty to only 1.4%-points and achieves a CO$_2$ avoidance cost of $60.3/ton, which is $33.5/ton below the cost of conventional post-combustion CO$_2$ capture with an energy penalty of 8.1%-points. Due to the added natural gas firing after the CLC reactors, this plant only avoids 52.4% of CO$_2$ emissions. However, given the uncertainty regarding CO$_2$ pricing, low-cost partial CO$_2$ capture could be a good strategy in the medium term. The proposed partial capture CLC plant is well suited to such a strategy because its LCOE is only $10.4/MWh higher than an unabated NGCC plant and $17/MWh lower than an NGCC plant with post-combustion capture.

High CO$_2$ avoidance can be achieved by firing the added combustor with clean hydrogen, but this increases the fuel cost. To increase CO$_2$ avoidance to 94.9%, the H$_2$ firing increases the CO$_2$ avoidance cost to $96.3/ton when a hydrogen cost of $15.5/GJ is assumed. Advanced heat integration could reduce the CO$_2$ avoidance cost to $90.3/ton by further reducing the energy penalty to only 0.6%-points. Firing with hydrogen from an advanced reforming process such as membrane-assisted autothermal reforming will result in CO$_2$ avoidance costs similar to that of the post-combustion benchmark. However, a dedicated
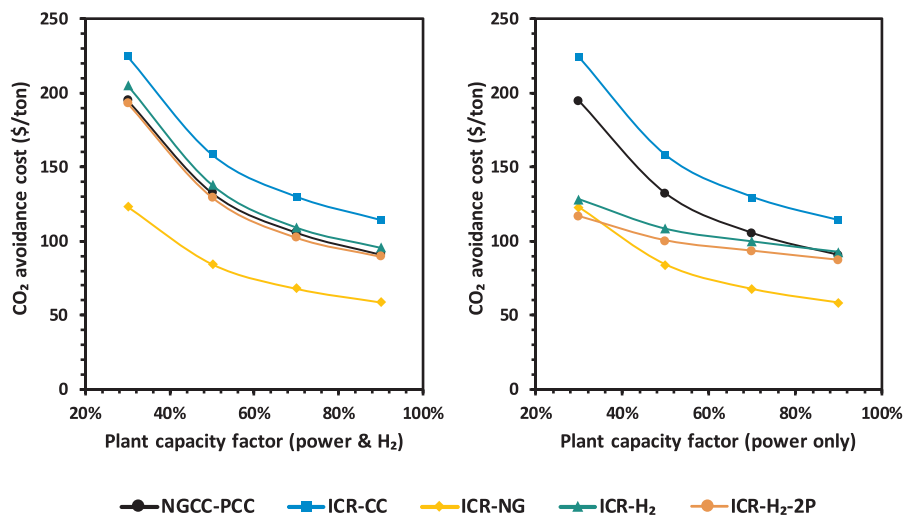

Fig. 13. Sensitivity of the CO$_2$ avoidance cost to capacity factor of both the power and hydrogen plants (left) and of the power plant only (right).
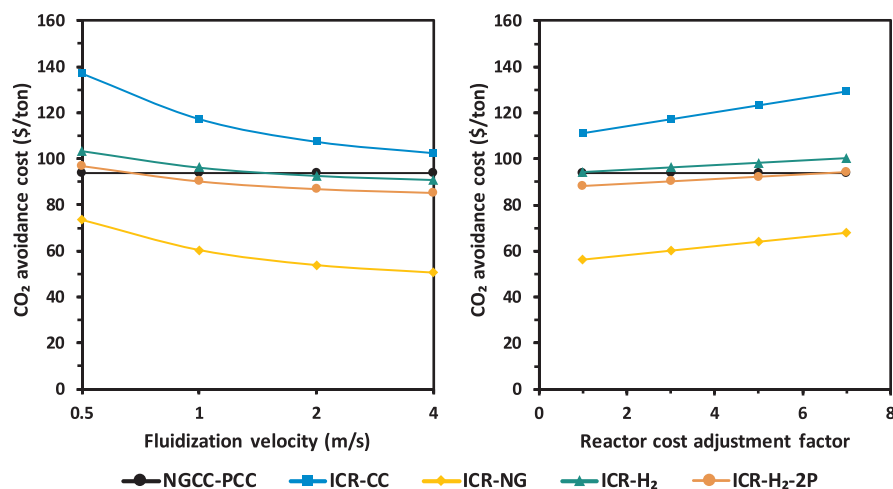
Fig. 14. Sensitivity of the CO_2 avoidance cost to important assumptions in the reactor capital cost calculation: the fluidization velocity used to determine the number of reactors required and the cost adjustment factor used to account for the complex internal structure of the ICR as well as downstream gas-particle separation equipment.

advanced reforming plant efficiently integrated into the power plant can undercut post-combustion CO_2 capture. A viable path forward is, therefore, to deploy CLC plants with added firing using natural gas and retrofit the plant later for added firing with hydrogen when CO_2 prices reach very high levels.

The added combustor presents some technical risk, but it could also bring substantial benefits in terms of NOx reduction over a range of plant loads. In general, load following operation could emerge as a strength of the CLC plant with added firing because part-load operation will reduce the firing temperature, reducing the reliance on the added combustor and thereby increasing the CO_2 avoidance. A load following CLC plant with added hydrogen firing operated at a low capacity factor becomes particularly attractive when the hydrogen production process can continue operating at a high capacity factor. This would require a hydrogen market to absorb clean hydrogen produced during times when the power plant must ramp down.

Using the added firing configuration, CLC can therefore play an important role in a future power system that is increasingly reliant on clean-burning natural gas. Further scale-up and demonstration of the ICR concept for CLC applications is recommended.

CRediT authorship contribution statement

Mohammed N. Khan: Methodology, Formal analysis, Investigation, Writing - original draft. **Paolo Chiesa:** Methodology, Formal analysis, Investigation, Writing - review & editing. **Schalk Cloete:** Conceptualization, Methodology, Formal analysis, Investigation, Writing - review & editing, Supervision, Funding acquisition. **Shahriar Amini:** Writing - review & editing, Supervision, Project administration, Funding acquisition.

Declaration of Competing Interest

The authors declare that they have no known competing financial interests or personal relationships that could have appeared to influence the work reported in this paper.

Acknowledgment

References

[1] Oceanography SI of. The Keeling Curve | A daily record of atmospheric carbon dioxide from Scripps Institution of Oceanography at UC San Diego 2019. https://scripps.ucsd.edu/programs/keelingcurve/ (accessed May 27, 2019).

[2] IEA. World Energy Outlook. Int Energy Agency 2019.

[3] IPCC. Global warming of 1.5°C. Intergov Panel Clim Chang 2018.

[4] Diego ME, Bellas J-M, Pourkashanian M. Techno-economic analysis of a hybrid CO2 capture system for natural gas combined cycles with selective exhaust gas re-circulation. Appl Energy 2018;215:778–91. https://doi.org/10.1016/J.APENERGY.2018.02.066.

[5] Sanchez Fernandez E, Goetheer ELV, Manzolini G, Macchi E, Rezvani S, Vlugt TJH. Thermodynamic assessment of amine based CO2 capture technologies in power plants based on European Benchmarking Task Force methodology. Fuel 2014;129:318–29. https://doi.org/10.1016/J.FUEL.2014.03.042.

[6] Ystad PAM, Bolland O, Hillestad M. NGCC and hard-coal power plant with CO2 capture based on absorption. Energy Proc 2012;23:33–44. https://doi.org/10.1016/J.EGYPRO.2012.06.019.

[7] Ishida M, Zheng D, Akehata T. Evaluation of a chemical-looping-combustion power-generation system by graphic exergy analysis. Energy 1987;12:147–54. https://doi.org/10.1016/0360-5442(87)90119-8.

[8] Ekström C, Schwendig F, Biede O, Franco F, Haupt G, de Koeijer G, et al. Techno-economic evaluations and benchmarking of pre-combustion CO2 capture and oxy-fuel processes developed in the European ENCAP project. Energy Proc 2009;1:4233–40. https://doi.org/10.1016/j.egypro.2009.02.234.

[9] Baek J-I, Ryu J, Lee JB, Eom T-H, Kim K-S, Yang S-R, et al. Highly attrition resistant oxygen carrier for chemical looping combustion. Energy Proc 2011;4:349–55. https://doi.org/10.1016/J.EGYPRO.2011.01.061.

[10] Khan MN, Shamim T. Thermodynamic screening of suitable oxygen carriers for a three reactor chemical looping reforming system. Int J Hydrogen Energy 2017;42:15745–60. https://doi.org/10.1016/J.IJHYDENE.2017.05.037.

[11] Pröll T, Kolbitsch P, Bolhàr-Nordenkampf J, Hofbauer H. A novel dual circulating fluidized bed system for chemical looping processes. AIChE J 2009;55:3255–66. https://doi.org/10.1002/aic.11934.

[12] Bao J, Li Z, Sun H, Cai N. Continuous test of ilmenite-based oxygen carriers for chemical looping combustion in a dual fluidized bed reactor system. Ind Eng Chem Res 2013;52:14817–27. https://doi.org/10.1021/ie4025209.

[13] Kronberger B, Johansson E, Löffler G, Mattisson T, Lyngfelt A, Hofbauer H. A two-compartment fluidized bed reactor for CO2 capture by chemical-looping combustion. Chem Eng Technol 2004;27:1318–26. https://doi.org/10.1002/ceat.200402137.

[14] Linderholm C, Abad A, Mattisson T, Lyngfelt A. 160 h of chemical-looping combustion in a 10 kW reactor system with a NiO-based oxygen carrier. Int J Greenh Gas Control 2008;2:520–30. https://doi.org/10.1016/J.IJGGC.2008.02.006.

[15] Kolbitsch P, Bolhàr-Nordenkampf J, Pröll T, Hofbauer H. Operating experience with chemical looping combustion in a 120 kW dual circulating fluidized bed (DCFB) unit. Int J Greenh Gas Control 2010;4:180–5. https://doi.org/10.1016/J.IJGGC.2009.09.014.

[16] Zaabout A, Cloete S, Johansen ST, van Sint Annaland M, Gallucci F, Amini S. Experimental demonstration of a novel gas switching combustion reactor for power production with integrated CO2 capture. Ind Eng Chem Res 2013;52:14241–50. https://doi.org/10.1021/ie401810n.

[17] Zhao Z, Chen T, Ghoniem AF. Rotary bed reactor for chemical-looping combustion with carbon capture. Part 1: Reactor design and model development. Energy Fuels 2013;27:327–43. https://doi.org/10.1021/ef3014103.

[18] Kuramoto M, Furusawa T, Kunii D. Development of a new system for circulating fluidized particles within a single vessel. Powder Technol 1985;44:77–84. https://doi.org/10.1016/0032-5910(85)85024-5.

[19] Barisano D, Canneto G, Nanna F, Alvino E, Pinto G, Villone A, et al. Steam/oxygen biomass gasification at pilot scale in an internally circulating bubbling fluidized bed reactor. Fuel Process Technol 2016;141:74–81. https://doi.org/10.1016/J.FUPROC.2015.06.008.

[20] Li P, Wang T, Liu Y, Zhang Q, Li Q, Xiong R, et al. CFD simulation of the

hydrodynamic behavior in an internally circulating fluidized bed reactor for producing polysilicon granules. Powder Technol 2017;311:496–505. https://doi.org/10.1016/J.POWTEC.2017.01.068.

[21] Zaabout A, Cloete S, Amini S. Innovative internally circulating reactor concept for chemical looping-based CO2 capture processes: hydrodynamic investigation. Chem Eng Technol 2016;39:1413–24. https://doi.org/10.1002/ceat.201500222.

[22] Cloete S, Zaabout A, Amini S. The Internally Circulating Reactor (ICR) concept applied to pressurized chemical looping processes. Energy Proc. 2017;114:446–57. https://doi.org/10.1016/J.EGYPRO.2017.03.1187.

[23] Osman M, Zaabout A, Cloete S, Amini S. Internally circulating fluidized-bed reactor for syngas production using chemical looping reforming. Chem Eng J 2018. https://doi.org/10.1016/j.cej.2018.10.013.

[24] Osman M, Zaabout A, Cloete S, Amini S. Mapping the operating performance of a novel internally circulating fluidized bed reactor applied to chemical looping combustion. Fuel Process Technol 2020;197:106183https://doi.org/10.1016/j.fuproc.2019.106183.

[25] Naqvi R, Bolland O. Multi-stage chemical looping combustion (CLC) for combined cycles with CO2 capture. Int J Greenh Gas Control 2007;1:19–30. https://doi.org/10.1016/S1750-5836(07)00012-6.

[26] Hassan B, Ogidiama OV, Khan MN, Shamim T. Energy and exergy analyses of a power plant with carbon dioxide capture using multistage chemical looping combustion. J Energy Resour Technol 2016;139:032002https://doi.org/10.1115/1.4035057.

[27] Petriz-Prieto MA, Rico-Ramirez V, Gonzalez-Alatorre G, Gómez-Castro FI, Diwekar UM. A comparative simulation study of power generation plants involving chemical looping combustion systems. Comput Chem Eng 2016;84:434–45. https://doi.org/10.1016/j.compchemeng.2015.10.002.

[28] Porrazzo R, White G, Ocone R. Techno-economic investigation of a chemical looping combustion based power plant. Faraday Discuss 2016;192:437–57. https://doi.org/10.1039/C6FD00033A.

[29] Zerobin F, Pröll T. Potential and limitations of power generation via chemical looping combustion of gaseous fuels. Int J Greenh Gas Control 2017;64:174–82. https://doi.org/10.1016/j.ijggc.2017.07.011.

[30] Cloete JH, Khan MN, Cloete S, Amini S. Simulation-based design and economic evaluation of a novel internally circulating fluidized bed reactor for power production with integrated CO2 capture. Processes 2019;7:723. https://doi.org/10.3390/pr7100723.

[31] Khan MN, Cloete S, Amini S. Efficiency improvement of chemical looping combustion combined cycle power plants. Energy Technol 2019;1900567. https://doi.org/10.1002/ente.201900567.

[32] Gas Turbine World 2016-17 Handbook. vol. 32. Pequot Publishing; 2016.

[33] Chiesa P, Macchi E. A thermodynamic analysis of different options to break 60% electric efficiency in combined cycle power plants. J Eng Gas Turbines Power 2004;126:770–85. https://doi.org/10.1115/1.1771684.

[34] Thermoflow. Thermoflex V26 user guide. Southborough, MA, USA: 2017.

[35] Rao AB, Rubin ES. A technical, economic, and environmental assessment of amine-based CO2 capture technology for power plant greenhouse gas control. Environ Sci Technol 2002;36:4467–75. https://doi.org/10.1021/es0158861.

[36] Cavaliere A, De Joannon M. Mild combustion. Prog Energy Combust Sci 2004;30:329–66. https://doi.org/10.1016/j.pecs.2004.02.003.

[37] Khan MN, Shamim T. Investigation of hydrogen generation in a three reactor chemical looping reforming process. Appl Energy 2016;162:1186–94. https://doi.org/10.1016/J.APENERGY.2015.08.033.

[38] IEAGHG. Oxy-Combustion Turbine Power Plants 2015/05. 2015.

[39] U.S. Department of Energy - National Energy Technology Laboratory. Cost and Performance Baseline for Fossil Energy Plants Volume 3c: Natural Gas Combined Cycle at Elevation 2011;3c:167.

[40] Turton R, Bailie R, Whiting W, Shaeiwitz J. Analysis, synthesis and design of chemical processes. 2008.

[41] Cloete S, Khan MN, Amini S. Economic assessment of membrane-assisted autothermal reforming for cost effective hydrogen production with CO2 capture. Int J Hydrogen Energy 2019;44:3492–510. https://doi.org/10.1016/j.ijhydene.2018.12.110.

[42] Khan MN, Shamim T. Techno-economic assessment of a chemical looping reforming combined cycle plant with iron and tungsten based oxygen carriers. Int J Hydrogen Energy 2019;44:11525–34. https://doi.org/10.1016/J.IJHYDENE.2019.03.109.

[43] Khan MN, Shamim T. Techno-economic assessment of a plant based on a three reactor chemical looping reforming system. Int J Hydrogen Energy 2016;41:22677–88. https://doi.org/10.1016/J.IJHYDENE.2016.09.016.

[44] Peters MS, Timmerhaus KD. Plant Desing and Economics for Chemical Engineers. 1991.

[45] European Union Natural Gas Import Price n.d. https://ycharts.com/indicators/europe_natural_gas_price (accessed May 28, 2019).

[46] Nazir SM, Cloete S, Bolland O, Amini S. Techno-economic assessment of the novel gas switching reforming (GSR) concept for gas-fired power production with integrated CO2 capture. Int J Hydrogen Energy 2018;43:8754–69. https://doi.org/10.1016/J.IJHYDENE.2018.02.076.

[47] Cekirge HM, Erturan S. Modified levelized cost of electricity or energy, MLOCE and modified levelized avoidable cost of electricity or energy, MLACE and decision making. Am J Mod Energy 2019;5:1https://doi.org/10.11648/J.AJME.20190501.11.

[48] Medrano JA, Spallina V, Van Sint Annaland M, Gallucci F. Thermodynamic analysis of a membrane-assisted chemical looping reforming reactor concept for combined H2 production and CO2 capture. Int J Hydrogen Energy 2014;39:4725–38. https://doi.org/10.1016/j.ijhydene.2013.11.126.

[49] Nazir SM, Cloete JH, Cloete S, Amini S. Gas switching reforming (GSR) for power generation with CO2 capture: process efficiency improvement studies. Energy 2019;167:757–65. https://doi.org/10.1016/J.ENERGY.2018.11.023.

[50] Gülen SC. Gas Turbines for Electric Power Generation. Cambridge University Press; 2019. https://doi.org/10.1017/9781108241625.

[51] Rubin ES, Davison JE, Herzog HJ. The cost of CO2 capture and storage. Int J Greenh Gas Control 2015;40:378–400. https://doi.org/10.1016/J.IJGGC.2015.05.018.

[52] Cloete S, Hirth L. Flexible power and hydrogen production: finding synergy between CCS and variable renewables. Energy 2020;192:116671https://doi.org/10.1016/j.energy.2019.116671.